HiSST: International Conference on
High-Speed Vehicle Science Technology

26–29 November 2018, Moscow, Russia

Analysis of Porous Materials for Transpiration Cooled Heat Flux Sensor Development

Fabian Hufgard[1], Stefan Löhle[2], Tobias Hermann[3], Sven Schweikert[4], Matthew McGilvray[5], Jens von Wolfersdorf[6], Johan Steelant[7], Stefanos Fasoulas[8]

Abstract

The Non-Integer System Identification (NISI) method is an useful tool for the determination of surface heat flux from in-depth temperature data even in transpiration cooled environments. Recently it was demonstrated that in these transpiration cooled environments the surface heat flux can be determined using a measurement of the plenum pressure changes in the gas reservoir at the rear side of the porous structure for the Non-Integer System Identification (NISIp). This paper presents fundamental experiments required for the identification of susceptibilities with respect to the thermophysical and fluid properties. Test results with two different porous materials are compared: zirconium diboride and carbon/carbon. The experimental setup for both systems and the respective resulting impulse responses over varying coolant mass flows are presented and discussed in this paper. It was found that the pressure impulse responses of the ZrB_2 system is more sensitive to coolant mass flow rate changes than the C/C system with respect to both response time and amplitude pressure. However, the absolute response time of the C/C system was significantly shorter for all tested flow rates.

Keywords: *heat flux sensor, porous material, transpiration cooled environment, impulse response*

Nomenclature

Latin

A – Porous material's outblowing area
a – Thermal diffusivity
c_p – Heat capacity
$D^{n/2}$ – (Non-integer) derivation operator
H – Transfer function
h_v – Volumetric heat transfer coefficient
K_D – Permeability coefficient
K_F – Permeability coefficient
$\dot{m}$ – Mass flow
p – Pressure
q – Heat flux
q_0 – Surface heat flux
R – Specific gas constant for an ideal gas

[1]*PhD student, High Enthalpy Flow Diagnostics Group (HEFDiG), Institute of Space Systems, Stuttgart, Germany, hufgard@irs.uni-stuttgart.de*
[2]*Research scientist, Group leader HEFDiG, Institute of Space Systems, Stuttgart, Germany, loehle@irs.uni-stuttgart.de*
[3]*Post-doctoral research assistant, Hypersonics group, Oxford Thermofluids Institute, Oxford, United Kingdom, tobias.hermann@eng.ox.ac.uk*
[4]*PhD student, Institute of Aerospace Thermodynamics, Stuttgart, Germany, sven.schweikert@itlr.uni-stuttgart.de*
[5]*Associate professor, Hypersonics group, Oxford Thermofluids Institute, Oxford, United Kingdom, matthew.mcgilvray@eng.ox.ac.uk*
[6]*Professor, Institute of Aerospace Thermodynamics, Stuttgart, Germany, jens.vonwolfersdorf@itlr.uni-stuttgart.de*
[7]*Senior research scientist, ESA-ESTEC, Flight Vehicles and Aerothermodynamics Engineering Section, Noordwijk, Netherlands, johan.steelant@esa.int*
[8]*Professor, Director Institute of Space Systems, Stuttgart, Germany, fasoulas@irs.uni-stuttgart.de*

s – Laplace variable
T – Temperature
T_0 – Initial temperature
t – Time
v – Darcy velocity
x – Coordinate

Greek

α_n – NISI parameter
β_n – NISI parameter
λ – Thermal conductivity
μ – Viscosity
ρ – Density
Φ – Porosity

Subscripts

cal – Calibration
f – Fluid
pl – Plenum
s – Solid
sim – Simulation
tc – Thermocouple

1. Introduction

In aerospace engineering applications, components can be subject to extreme surface heat fluxes. Examples of this are heat shields for reentry vehicles or the internal wall structures of combustion chambers for rockets or (sc)ramjets [1–3]. In order to maintain structural integrity, active cooling is necessary for some applications. One such technology that has become more popular in the last decades is transpiration cooling. Here, a gaseous or liquid coolant is fed through the wall, which consists of a porous material, into the hot gas region. This has two effects. Firstly, the wall is actively cooled by the coolant, where the thermal energy is fed back into the hot gas region. Secondly, the coolant acts like an additional heat shield by forming a layer of comparatively cold gas between wall and hot gas. The second effect is not an actual cooling effect in the literal sense, but rather a reduction of the surface heat flux, which is causing the wall to heat up in the first place. A detailed description of this process can be found in [4] and references therein.

Significant improvement in the design of transpiration cooled applications requires a thorough characterization of the transpiration cooling by distinct measurements of temperatures and pressures. One essential value is the surface heat flux to which the material is exposed. Measurement of surface heat flux is still a challenging endeavour. One method, which has been developed by the High Enthalpy Flow Diagnostics Group (HEFDiG) at the Institute of Space Systems of the University of Stuttgart is the Non-Integer System Identification (NISI). Here, the basic idea is to characterize the respective sensor system entirely by using non-destructive testing of the actual hardware. A single calibrated temperature sensor suffices for the inverse determination of surface heat flux without a detailed knowledge of thermophysical properties and geometry of the sensor [5, 6]. The NISI method has been enhanced to the data analysis for transpiration cooled environments [7]. However, boreholes can decrease the structural performance. Also, glueing the thermocouple into the porous material implies uncertainties regarding flow field disruption around the spot of the temperature measurement itself. Although this is taken into account by NISI it can be disadvantageous for the cooling performance.

It was shown in a previous publication that for transpiration cooled systems subject to a constant coolant mass flow, the plenum pressure change is sensitive to the surface heat flux. Therefore, the NISI method can be applied using the measured plenum pressure profile [8]. The NISI method's pressure-based alteration NISIp appears to be a promising foundation to the development of a novel heat flux sensor. A major advantage of this method is that the porous material itself remains untouched, i.e. no boreholes for thermocouples. The sensor measuring the plenum pressure does not interact with the flow field in the porous wall, which would affect the heat flux. One puzzle piece in the development of a NISIp based heat flux sensor is the comprehension of the impact of sensor geometry, coolant mass flow rate and individual material parameters on a sensor's sensitivity.

In this paper the basic principles of the NISIp method are reviewed and an experimental setup for fundamental investigations is explained. The analysis results of two measurement campaigns with a transpiration cooled porous zirconium diboride (ZrB_2) and carbon/carbon (C/C) sample are presented, compared and discussed.

2. Theoretical Approach and Methodology

2.1. Non-Integer System Identification

The approach of the NISI method and its alteration NISIp is described in detail in several publications (see e.g., [5,9,10]). The NISI approach is founded on the one-dimensional heat equation with constant thermophysical properties, as sketched in Fig. 1. This problem can be expressed in the differential equation:

$$\frac{\partial T}{\partial t}(x,t) = \frac{\lambda}{\rho c_p}\frac{\partial^2 T}{\partial x^2}(x,t) \ , \qquad (x,t) \geq 0 \tag{1a}$$

subject to the boundary conditions

$$q(0,t) = q_0(t) = -\lambda \frac{\partial T}{\partial x} \ , \qquad t \geq 0 \tag{1b}$$

$$\lim_{x\to\infty} T(x,t) = T_0 \ , \qquad t > 0 \tag{1c}$$

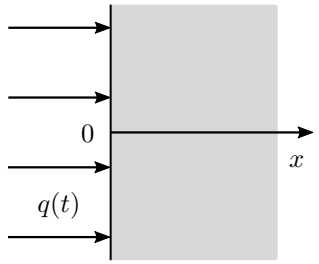

Fig. 1 1D semi-infinite heat conduction problem

and initial condition

$$T(x,0) = T_0 \ , \qquad x \geq 0 \ . \tag{1d}$$

Here ρ, c_p, and λ are the density, heat capacity, and heat conductivity of the material, respectively; T is the temperature, T_0 the initial temperature; x is the spatial coordinate of the one dimension; q is the heat flux and q_0 the net surface heat flux. Eq. 1a can be solved using a Laplace transformation yielding the ordinary differential equation

$$\frac{\mathrm{d}^2 \bar{T}(x,s)}{\mathrm{d}x^2} - \frac{s}{a}\bar{T}(x,s) = 0 \tag{2}$$

with the Laplace variable s and the thermal diffusivity $a = \lambda/(\rho c_p)$. The solution using an exponential approach leads to

$$\bar{T}(x,s) = K_1(s)e^{-x\sqrt{s/a}} + K_2(s)e^{x\sqrt{s/a}} \ . \tag{3}$$

The constants K_1 and K_2 are defined by the boundary conditions of the problem. For a semi-infinite heat conduction problem, the parameter $K_2 = 0$ and the solution of the problem in the Laplace domain is

$$H(x,s) = \frac{\bar{T}(x,s)}{\bar{q}_0(s)} = \frac{1}{\sqrt{s}\sqrt{\lambda\rho c_p}} e^{-x\sqrt{s/a}} \ . \tag{4}$$

Eq. 4 indicates that the problem can be abstracted as sketched in Fig. 2. The surface heat flux signal $\bar{q}_0(s)$ is transferred by a function $H(x,s)$ to the temperature signal $\bar{T}(x,s)$. For problems with higher complexity (i.e., without the assumption of one-dimensional semi-infinite heat conduction), this transfer function can be written more generally as the expansion [5]

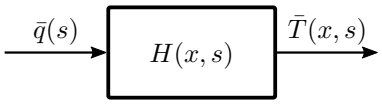

Fig. 2 Theoretical system consideration of the heat conduction problem

$$H(x,s) = \frac{\bar{T}(x,s)}{\bar{q}_0(s)} = \frac{1}{\sqrt{s}\sqrt{\lambda\rho c_p}} \sum_{n=0}^{\infty} \frac{(-1)^n s^{n/2} x^n}{(\lambda/(\rho c_p))^{n/2} n!} \ . \tag{5}$$

The order of the exponent of s in the Laplace domain is the order of the differentiation in the time domain. According to the extension of this model function by Battaglia et al. [5], the general transfer function at a given position $x = d$ in the Laplace domain is of the form

$$H(s) = \frac{\sum_{n=L_0}^{L\to\infty} \beta_n s^{n/2}}{\sum_{n=M_0}^{M\to\infty} \alpha_n s^{n/2}} \tag{6}$$

which, in the time domain, corresponds to

$$\sum_{n=M_0}^{M} \alpha_n D^{n/2} T_{tc}(t) = \sum_{n=L_0}^{L} \beta_n D^{n/2} q_0(t) \qquad \text{with} \qquad \alpha_{M_0} = 1 \ , \tag{7}$$

where $T_{tc}(t)$ is the temperature profile at the measurement spot $x = d$. As can be seen from Eq. 7, the system is characterized for $x \geq 0$ by the model parameters α_n and β_n and the (non-integer) derivation D of the order $n/2$.

For the calibration of a sensor system, a known heat flux is applied to the surface while the temperature is measured. The identification of the unknown parameters α_n and β_n is solved by rebuilding the measured temperature signal using a least-squares method. The implementation of this approach in usable computer code is described in detail by Battaglia et al. [5] and Gardarein et al. [10]. The non-integer derivatives are calculated using an algorithm by Grünwald and Letnikov as given in [11]. The identified set of parameters is used to calculate the temperature profile for a numerical implementation of a Dirac impulse, that is a heat flux with an amplitude of $1\,\mathrm{W/m^2}$ and a duration of one time step. The resulting temperature profile represents the system's impulse response, which fully characterizes the given system [12]. The impulse response exhibits a sensor system's temporal behaviour, i.e. its sensitivity.

2.2. Pressure-Based Non-Integer System Identification

It turns out that, given a constant coolant mass flow, the plenum pressure reading shows a similar temporal response to a heat flux signal as the temperature reading. The corresponding heat conduction problem is sketched in Fig. 3. It proved to be applicable to identify such a system using the same NISI Eq. 7 and replacing the temperature signal with the pressure reading [8]. The resulting pressure-based alteration of the NISI method is called NISIp. The related NISIp equation, which is also used for this work, reads

$$\sum_{n=M_0}^{M} \alpha_n D^{n/2} p_{pl}(t) = \sum_{n=L_0}^{L} \beta_n D^{n/2} q_0(t) \qquad \text{with} \qquad \alpha_{M_0} = 1 \ . \tag{8}$$

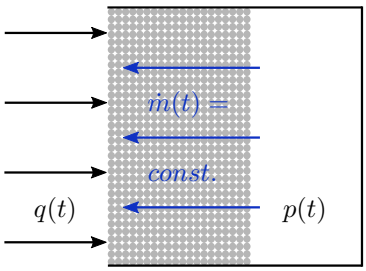

Fig. 3 Heat conduction problem for a transpiration cooled porous material

A mathematically consistent explanation for the applicability of Eq. 8 was not yet developed. However, a rather phenomenological explanation can be given by the fundamental equations of transpiration cooled environments. The thesis introduced by Löhle et al. [8] is that an increase in pressure is actually the effect of local heating of the solid close to the surface. Because the gas mass flow through the porous media is held constant and the gas is transparent to the laser light, heating the surface with laser radiation basically results in a temperature increase of the solid surface. The heat is conducted into the material and the gas flow consumes some of this heat while passing toward the surface. This line of argument is strengthened by considering the problem-associated energy equations, which are represented by a coupled set of partial differential equations for solid and fluid. According to Nield et al. [13] these equations are given for one spatial dimension by

$$\frac{\partial T_s}{\partial t}(x,t) = a_s \frac{\partial^2 T_s}{\partial x^2}(x,t) + \frac{h_v}{(1-\Phi)\rho_s c_{p,s}}(T_f(x,t) - T_s(x,t)) \ , \qquad (x,t) \geq 0 \tag{9}$$

for the solid and

$$\frac{\partial T_f}{\partial t}(x,t) + v\frac{\partial T_f}{\partial x}(x,t) = a_f \frac{\partial^2 T_f}{\partial x^2}(x,t) + \frac{h_v}{\Phi\rho_f c_{p,f}}(T_f(x,t) - T_s(x,t)) \ , \qquad (x,t) \geq 0 \tag{10}$$

for the fluid. The porous material-related properties are described by the porosity Φ and the volumetric heat transfer coefficient h_v. ρ is the density and c_p the specific heat capacity. The indices s and f denote solid and fluid, respectively. In combination with the temperature difference between solid and fluid $(T_s - T_f)$, h_v defines the amount of heat that is transferred between solid and fluid. A relation is thus needed that correlates the pressure difference to the temperature of the solid.

The fluid velocity is the driving parameter for the internal heat transfer in the porous material and is described by v, the superficial or Darcy velocity. The associated pressure loss in porous media is commonly described by the Darcy–Forchheimer equation

$$\frac{\partial p}{\partial x}(x,t) = -\left(\frac{\mu_f(x,t)v(x,t)}{K_D} + \frac{\rho_f(x,t)v(x,t)^2}{K_F}\right) \quad , \qquad (x,t) \geq 0 \tag{11}$$

where μ_f is the fluid's viscosity and K_D and K_F are the material characteristic permeability coefficients [14]. Substitution of the Darcy velocity in Eq. 11 by the continuity equation $v = \dot{m}/(\rho_f A)$ and the density by ideal gas law $\rho_f = p/(RT_f)$, yields

$$p\frac{\partial p}{\partial x}(x,t) = -\left(\frac{\mu_f(x,t)\dot{m}RT(x,t)}{K_D A} + \frac{\dot{m}^2 RT(x,t)}{K_F A^2}\right) \quad , \qquad (x,t) \geq 0 \tag{12}$$

where R is the specific gas constant for an ideal gas and A the cross sectional area of the porous material. The temperature dependency of the viscosity can be described, for example, by a power law or the Sutherland formulation (i.e., $\mu_f(x,t) = \mu_f(T(x,t)) = \mu_{ref}(T(x,t)/T_{ref})^n$). Thus, in Eq. 12 the only two parameters that are a function of time and space are the pressure on the one side and the temperature on the other, where the correlation between the two is proportional [8]. The effect has also been observed by Hermann et al. [15].

3. Experimental Setup

In this paper, the results of investigations of two different porous materials, zirconium diboride (ZrB_2) and carbon/carbon (C/C), are compared. Conceptionally the respective setups for both test campaigns were equal. The square-shaped porous sample was mounted within a metal sample holder and sealed at the edges. A gaseous coolant was fed through a mass flow controller into a plenum behind the porous sample. After transpiring through the porous sample the coolant exited toward ambient conditions. For both campaigns, the gas supply pressure was 8 bar, which is consequently the maximum achievable plenum pressure. The transient plenum pressure is measured using a commercial gauge. Radiative heating is provided by a diode laser (Laserline LDM 500-100). The laser wavelength is 980 nm and its power rise time is < 0.1 ms. The laser power is determined with the manufacturer's calibration information from the power setting. The focusing optics expanded the laser beam homogeneously into a square-shaped spot. In both experiments the radiated area was larger than the porous material's surface and thus overlapped it to all sides in order to minimise lateral conduction. Both the laser input power and the pressure signal were recorded with an oscilloscope (LeCroy 24Xs-A).

The partially sintered ZrB_2 sample was manufactured and the material properties, which are listed in Table 1, were characterized by the Department of Materials of Imperial College London. The given permeability properties were characterized by the Hypersonics Group at the Oxford Thermofluids Institute [16]. The sample's area was 32 x 32 mm^2 and it was 5 mm thick. In the measurement campaign with this sample, nitrogen was chosen as the coolant. It was controlled by a Bronkhorst 1 g/s mass flow controller. The pressure gauge used was a GEMS 3100 Series (0 - 40 bar). The volume of the plenum for these experiments was approximately $2 \cdot 10^{-4}$ m^3. A layer of cement was used as sealant and thermal insulation between the porous sample and the sample holder. The area of the laser spot was set to 68 x 68 mm^2.

The C/C sample was 50 x 50 mm^2 and it was 11.16 mm thick. It was manufactured at the German Aerospace Center (DLR) in Stuttgart and can be seen as reference material for ceramic matrix composites in aerospace applications [4, 20–23]. It was actually designed and used for surface heat flux measurements in a hot gas test facility at the Institute of Aerospace Thermodynamics (ITLR) of the University

Table 1 Material properties of the porous samples

	Φ / %	K_D / m²	K_F / m	λ / W/m/K	ρ / kg/m³	c_p / J/kg/K
ZrB_2	42	$2.44 \cdot 10^{-14}$ [16]	$8.86 \cdot 10^{-8}$ [16]	41.4	6080	437.6 [17]
C/C	12.4 [18]	$2.0 \cdot 10^{-13}$	$9.1 \cdot 10^{-9}$	1.75 [19]	1375	950 [19]

of Stuttgart [24]. One part of these experiments was the application of the NISIp method. The data recorded in the required laser calibration were used for the present investigation. The material parameters of the sample were characterised by ITLR and are listed in Table 1. The coolant used for these calibration measurements was air, which was controlled by a HFC-303, Teledyne-Hastings mass flow controller. The plenum pressure was recorded using a Newport Omega PAA33X-C-15. Here, the plenum volume was approximately $9 \cdot 10^{-4}$ m³. The porous C/C sample was edged by a copper lip using adhesive to seal the gap between the two materials. The laser heat load was homogeneously distributed over a 80 x 80 mm² area.

4. Results

In Fig. 4 the measured data of the calibration experiments for both investigated materials, ZrB_2 (left plot) and C/C (right plot) are shown. Relevant data for the calibration are the heat flux and the plenum pressure difference (Δp_{cal}) with respect to the steady state pressure at t = 0 s for the given coolant mass flow. The indicated coolant mass flows were held constant by the respective mass flow controller.

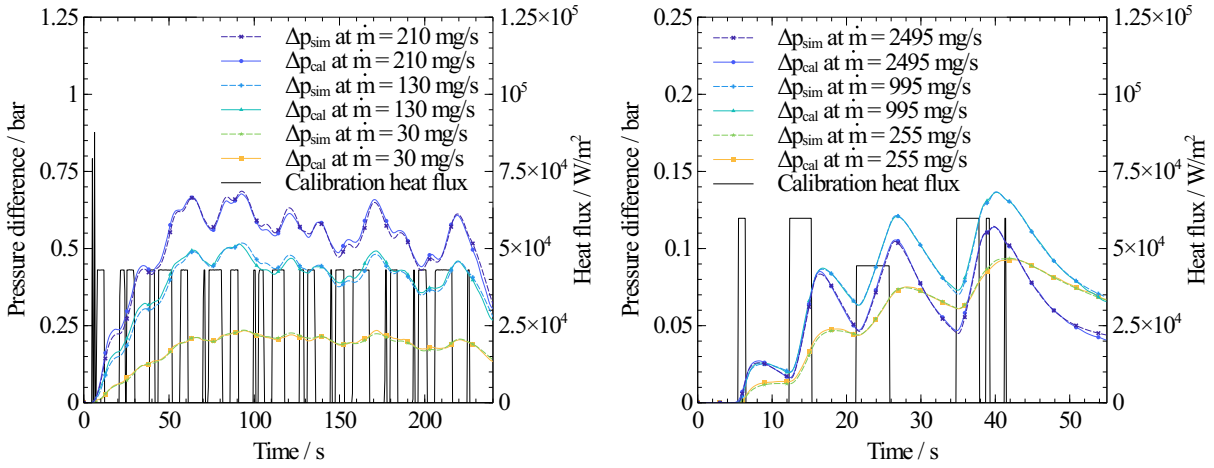

Fig. 4 For both transpiration cooling experiments with ZrB_2 (left) and C/C (right), the applied calibration heat flux, three exemplary calibration data sets (solid lines) and simulated pressure profiles resulting from the NISI identification step (dashed lines)

The heat flux profiles have been chosen randomly with a nominal heat flux of 43 kW/m² (ZrB_2) and 60 kW/m² (C/C). It can be observed in both plots of Fig. 4 that the pressure increases after the heat flux affects the surface. The ZrB_2 system appears to react slower, however. Whilst for the C/C sample even short pulses are well distinguishable by a measured plenum pressure change, the short pulses in the left plot hardly imply a noticeable effect. In the left plot of Fig. 4, the sensitivity and overall pressure gain increases with flow rate. As can be seen in the right plot, the overall pressure gain reaches a maximum at a flow rate of 995 mg/s and decreases from this point with increasing flow rates.

The calibration data are used for the identification of the NISIp parameters α_n and β_n (see Eq. 8). The least-squares fit (Δp_{sim}) of the identified parameter set are depicted as dashed lines in Fig. 4 for both

experiments. As can be seen, a good agreement between the NISIp-identification and the measurement data is obtained for both systems.

The transfer function is built between heat flux and pressure difference. The identified system for the example of the ZrB_2 sample at 130 mg/s mass flow results in

$$\begin{aligned}(D^{-0.5} + 19.51 + 7.21D^{0.5} + 566.63D + 94.72D^{1.5} - 326.31D^2 \\ +619.22D^{2.5} - 177.79D^3 + 2.65D^{3.5})p(t) \\ = (8.44 \cdot 10^{-4} - 2.40 \cdot 10^{-3}D^{0.5} + 2.40 \cdot 10^{-3}D - 7.09 \cdot 10^{-4}D^{1.5} - 4.6 \cdot 10^{-3}D^2 \\ +5.40 \cdot 10^{-3}D^{2.5} - 3.40 \cdot 10^{-3}D^3 + 1.20 \cdot 10^{-3}D^{3.5} - 2.40 \cdot 10^{-4}D^4 + 1.99 \cdot 10^{-5}D^{4.5})q(t)\end{aligned} \tag{13}$$

that is, nine parameters on the pressure side and ten parameters on the heat flux side were used to reproduce the measured pressure data (see Fig. 4). For the system identification of the other mass flows for the ZrB_2 experiments, the same polynomial order shown in Eq. 13 was used, resulting in each time different parameters (α_n and β_n). Analogously the polynomial order, which is shown in Eq. 14 for the example of the C/C sample at 995 mg/s mass flow, was used for the reproduction of the C/C pressure data.

$$\begin{aligned}(1 - 1.99D^{0.5} + 3.78D - 1.66D^{1.5} + 0.75D^2)p(t) \\ = (9.01 \cdot 10^{-7}D^{-0.5} - 3.23 \cdot 10^{-7} + 4.76 \cdot 10^{-8}D^{0.5} + 2.46 \cdot 10^{-9}D)q(t)\end{aligned} \tag{14}$$

Using this identified system, impulse responses were calculated for varying coolant mass flows for both experiments (see Fig. 5). Here, the required heat flux impulse was realised by the numerical implementation of a Dirac impulse. In this case this equals a heat flux with the amplitude of 1 W/m^2 and a duration of one time step, which was 0.4225 s in the ZrB_2 experiments and 0.0997 s in the C/C experiments. When applying a calibrated sensor system to a measurement scenario, the said procedure allows for the reconstruction of an unknown surface heat flux by measuring the pressure profile and deconvolve it with the respective calculated impulse response. In the measurement scenario the usage of the very same sensor system consisting of porous sample, plenum, pressure gauge and flow controller is required.

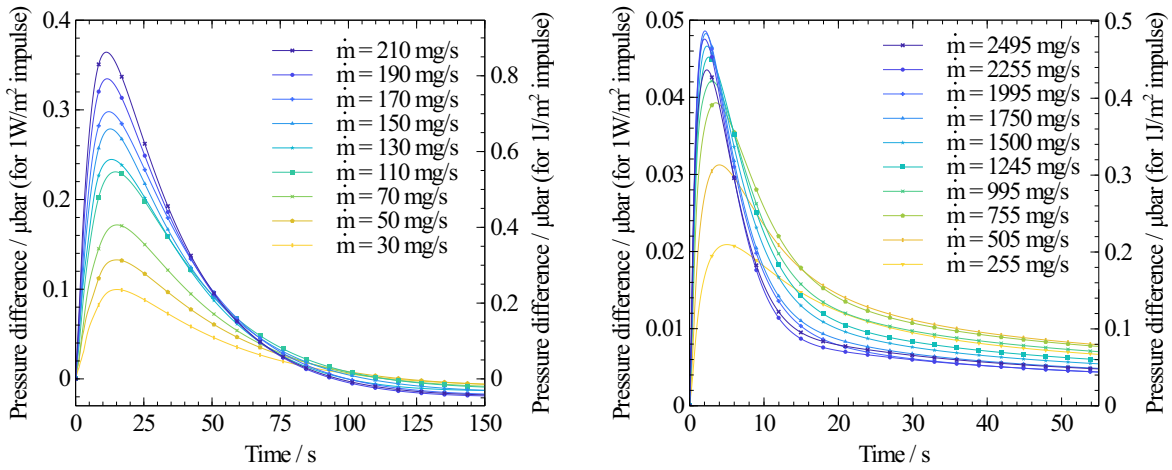

Fig. 5 Impulse responses for varying coolant mass flows calculated with the identified NISIp parameters and a 1 W/m^2 impulse (duration of one time step); the respective right ordinate gives the theoretical scale for an impulse of 1 J/m^2 for comparison between the two transpiration cooling experiments with ZrB_2 (left) and C/C (right)

For the transpiration cooling experiment with ZrB_2 (see left plot of Fig. 5), the impulse responses are lower magnitude for higher mass flows toward longer times, i.e. after about 100 s. This behaviour is consistent with the thesis introduced by Löhle et al. [8] that the pressure change is actually induced by

a temperature rise of the porous material. The reason for this is that the amount of heat absorbed by the coolant, i.e. the cooling of the porous material, increases with the flow rate. This results in a lower temperature of the porous material and thus plenum pressure. For the same ZrB_2 transpiration cooling experiment discussed in this work, the decrease of the porous material's temperature impulse response with increasing flow rates is presented in [15] for both perfused surfaces of the sample. On the other hand, the impulse responses' (max.) amplitudes increase with coolant mass flow. Also, the slope before and after the maximum becomes steeper. This means that a given system is, in terms of amplitude, more sensitive at higher flow rates, i.e. pressure increases faster at higher flow rates after a heat flux is introduced to the surface. Incidentally, this entails that higher flow rates are advantageous for solving the inverse heat conduction problem in a measurement scenario.

After a heat flux is applied to the surface, the temperature of both solid and fluid increases. This leads to an increased viscosity of the coolant inside the porous material, which decreases the flow rate through the sample temporarily. Assuming the ideal gas law and a constant plenum temperature, the plenum pressure change is a function of mass flow difference between flow controller and porous sample. Assuming further that the mass flow difference induced by a given surface heat flux is proportional to the mass flow rate itself, plenum pressure change is a function of the nominal flow rate (through the flow controller). This inflate effect counteracts the cooling effect and appears to be dominant toward shorter times, i.e. around the maximum of the impulse response, for the flow rate range tested in the measurement campaign with the ZrB_2 system.

The described behaviour (increasing flow rate leads to higher amplitude and lower value toward longer times) are also observable for the impulse responses in the right plot of Fig. 5 (C/C) for the mass flow rates between 505 and 1995 mg/s. The amplitude of the impulse response for 255 mg/s is the lowest of all curves and thus also follows the described behaviour, but it is not on top of all other curves toward longer times. The amplitude is highest for a mass flow of 1995 mg/s. For higher mass flows, the amplitudes decrease with increasing mass flow. This indicates that the cooling effect becomes dominant over the inflate effect and the impulse response becomes damped. The impulse response for 2495 mg/s is contrary to the general behaviour not the lowest toward longer times.

In order to compare the amplitude of the acquired impulse responses from both campaigns with each other, the respective impulses used for the calculation of the impulse response need to be similar. This is the case when the same (area specific) energy is introduced into the system, e.g. $1\,J/m^2$. This corresponds to rescaling the heat flux pulse by dividing by the length of one time step. Since the system is assumed to be linear, the calculated impulse responses can analogously be rescaled. The resulting scale is represented by the respective right ordinate in Fig. 5.

As can be seen from the normalised impulse responses in Fig. 6 for both ZrB_2 (left) and C/C (right), the maximum value of the impulse response is reached earlier for increasing flow rates. This means that the system has a faster response time at higher flow rates. For the C/C sample, the maximum pressure is reached after 2 - 6 s. Both observations are consistent with the results of Löhle et al. [8], where the investigated porous material was similar.

When comparing the speed of the two systems, i.e. duration until the impulse response reaches its amplitude, it becomes clear that the C/C system responds much quicker than the ZrB_2 system. A relatively thick sample with low thermal conductivity and thermal diffusivity distributes applied heat rather poorly. Therefore, the temperature response at the sample's back side (plenum side) is rather slow and weak. As the plenum pressure directly correlates to the temperature of the porous sample, a rather thin and thermally high conductive and diffusive sample intuitively appears advantageous for a quick pressure impulse response. The ZrB_2 sample is half as thick as the C/C sample. Also, the ZrB_2 sample's thermal conductivity is more than twenty times higher and its thermal diffusivity more than ten times ($15.6 \cdot 10^{-6}\,m^2/s$ for ZrB_2 vs. $1.3 \cdot 10^{-6}\,m^2/s$ for C/C). Nevertheless, the C/C sample is showing the faster response. A possible explanation is that the for a given heat pulse introduced to the surface, the solid temperature close to the surface and therefore also coolant viscosity increases more in a material with a low thermal diffusivity, which again could lead to a higher mass flow drop. Proving this correlation, however, is subject to future research. A potential bias is introduced by the thermal insulation between

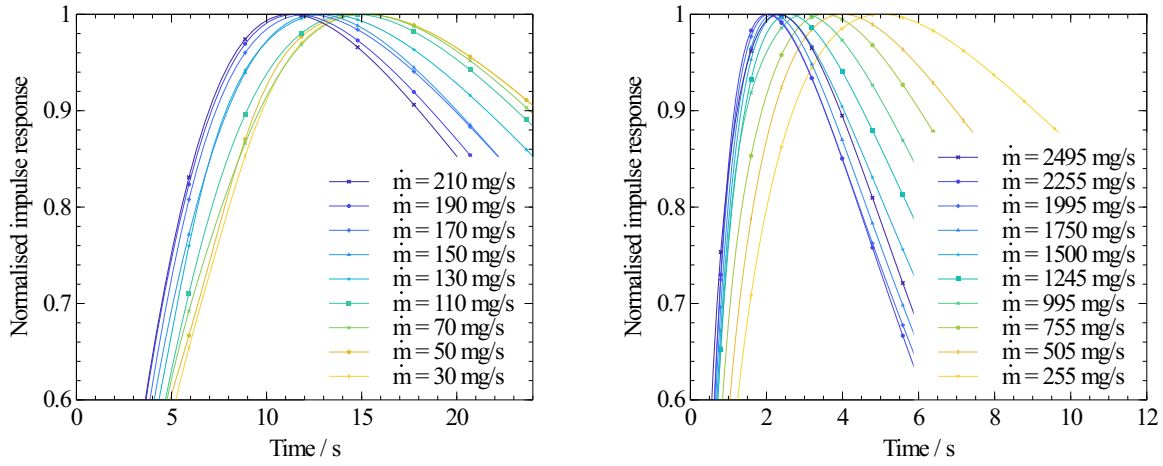

Fig. 6 Normalised impulse responses for varying coolant mass flows from the respective identified ZrB_2 (left) and C/C systems (right)

the ZrB_2 and the metal sample holder by a thermally low conducting cement, where the C/C sample was not particularly thermally insulated. Heat losses through the sample's sides would lead to a quicker decrease of solid temperature, which is directly proportional to the plenum pressure. As mentioned in Sec. 3, this effect was counteracted by radiating also the structure around the porous sample with the calibration laser.

As mentioned above, the plenum pressure change is a function of mass flow for a given plenum volume. In order to compare the sensitivity of the two systems with each other, the flow rate was normalised by division with the plenum volume. The plenum volume normalised flow rate is 0.15 - 1.05 kg/s/m^3 for the ZrB_2 experiment and 0.28 - 2.78 kg/s/m^3 for the C/C experiment, thus approximately 2.5 times higher for C/C. Here the difference in molar mass between air and nitrogen has been neglected. This indicates that besides a high flow rate, a small plenum volume is favourable for a quicker sensor system. In Fig. 7 the pressure amplitude is plotted over the plenum volume normalised flow rate. It can be observed that the pressure amplitudes are in the same order of magnitude for both experiments. The amplitude pressure change increases more rapidly for the ZrB_2 sample over the plenum volume normalised flow rate. Also it is increasing strictly monotonically, whereas the C/C impulse responses' amplitude pressure

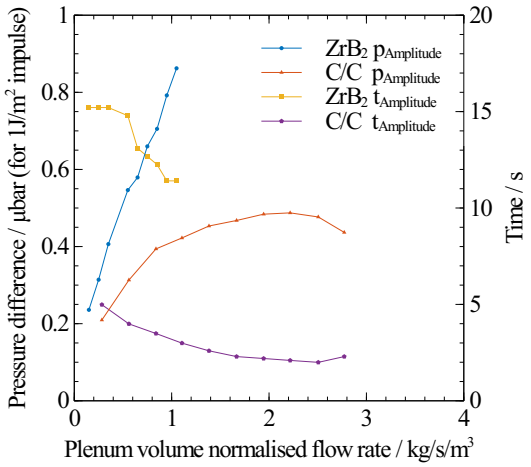

Fig. 7 Impulse responses' pressure amplitude and time until amplitude vs. plenum volume normalised flow rate

decreases for the normalised flow rates above 2.2 kg/s/m^3. A possible explanation is that the cooling effect becomes more dominant at higher flow rates, because the heat, which induces a temperature and thus coolant viscosity rise, gets absorbed and carried out of the system by the coolant faster than the plenum pressure is built up. Fig. 7 illustrates that the response time decreases with increasing normalised flow rate faster for the ZrB_2 system. In conclusion, the ZrB_2 system is more sensitive to flow rate changes than the C/C system with respect to both response time and amplitude pressure.

For the ZrB_2 tests the measurement campaign was conducted over the course of several days. It was observed after the campaign, that the respective first measurement of a day showed an odd behaviour, where the pressure profile decreased significantly over the course of the calibration measurement. This pertains for the measurement with a mass flow of 90 mg/s. The corresponding impulse response also showed odd behaviour and was left out consequently. A possible explanation is that after first tests due to thermal expansion some "cold" leakages have been closed. It is therefore recommended to preheat a given sample before the first test of a day.

5. Conclusion

NISIp is used for the development of a transpiration cooled heat flux sensor. Its basic applicability to pressure measurements has already been demonstrated in the past. This paper gives first insight into the current research for an optimum porous sample configuration. Two porous material samples have been investigated and compared in different setups. Besides the increased cooling for a higher coolant mass flow rate, a second mechanism has been found to significantly contribute to the temporal behaviour of the pressure impulse response shortly after an induced heat impulse. This effect causes the max. amplitudes of the impulse responses to increase with coolant mass flow rate. For this reason, especially the (plenum volume normalised) coolant mass flow rate influence the performance of the sensor system, which also includes the plenum, the flow controller and pressure gauge. A high flow rate and a small plenum volume are beneficial for this method. It was shown that the pressure impulse responses of the ZrB_2 system is more sensitive to flow rate changes than the C/C system with respect to both response time and amplitude pressure. However, the absolute response time of the C/C system was significantly shorter than for the ZrB_2 system for all tested flow rates. The exact impact of the geometry and the thermophysical properties of the used porous material will be investigated in the next steps using additional materials for comparison.

Acknowledgments

This work is partly funded through the ESA NPI Program under contract No. 4000121220/17/NL/MH. The authors thank Laura Larrimbe, Daniel Glymond and Luc Vandeperre from Imperial College London for providing the material samples and the respective thermophysical properties.

References

[1] R. N. Gupta. Aerothermodynamic analysis of stardust sample return capsule with coupled radiation and ablation. *Journal of Spacecraft and Rockets*, 37(4):507–514, July 2000.

[2] D. Preclik, D. Wiedmann, W. Oechslein, and J. Kretschmer. Cryogenic rocket calorimeter chamber experiments and heat transfer simulations. In *34th AIAA/ASME/SAE/ASEE Joint Propulsion Conference and Exhibit*, page 3440, 1998.

[3] R. Arnold. *Experimentelle Untersuchungen zur Filmkühlung in Raketenbrennkammern*. Cuvillier, 2008.

[4] H. Boehrk, O. Piol, and M. Kuhn. Heat balance of a transpiration-cooled heat shield. *Journal of Thermophysics and Heat Transfer*, 24(3):581–588, jul 2010.

[5] J.-L. Battaglia, O. Cois, L. Puigsegur, and A. Oustaloup. Solving an inverse heat conduction problem using a non-integer identified model. *International Journal of Heat and Mass Transfer*, 44:2671–2680, 2001.

[6] S. Loehle, J.-L. Battaglia, P. Jullien, B. van Ootegem, J. Couzi, and J.-P. Lasserre. Improvement of high heat flux measurements using a null-point calorimeter. *Journal of Spacecrafts and Rockets*, 45(1):76–81, 2007.

[7] S. Loehle and U. Fuchs. Heat flux calibration measurement using noninteger system identification method for cooled surfaces. *AIAA Journal of Thermophysics and Heat Transfer*, 25(2):213–217, 2011.

[8] S. Loehle, S. Schweikert, and J. von Wolfersdorf. Method for heat flux determination of a transpiration cooled wall from pressure data. *Journal of Thermophysics and Heat Transfer*, 30(3):567–572, 2016.

[9] S. Loehle, J.-L. Battaglia, J.-C. Batsale, O. Enouf, J. Dubard, and R.-R. Filtz. Characterization of a heat flux sensor using short pulse laser calibration. *Review of Scientific Instruments*, 78, 2007.

[10] J.-L. Gardarein, J.-L. Battaglia, and S. Loehle. Heat flux sensor calibration using noninteger system identification: Theory, experiment, and error analysis. *Review of Scientific Instruments*, 80(025103), 2009.

[11] I. Podlubny. *Fractional Differential Equations*. Academic Press, 1998.

[12] L. Ljung. *System Identification: Theory for the user*. Prentice Hall, 1987.

[13] D. A. Nield, A. Bejan, et al. *Convection in porous media*, volume 3. Springer, 2006.

[14] M. Innocentini, V. R. Salvini, J. R. Coury, and V. C. Pandolfelli. Permeability of ceramic foams. *American Ceramic Society Bulletin*, 78(9):78–84, 1999.

[15] T. Hermann, M. McGilvray, H. S. Ifti, F. Hufgard, and S. Loehle. Fluid-solid heat exchange in porous media for transpiration cooling systems. In *2019 AIAA SciTech Forum*. American Institute of Aeronautics and Astronautics, January 2019. submitted.

[16] H. S. Ifti, T. Hermann, and M. McGilvray. Flow characterisation of transpiring porous media for hypersonic vehicles. In *22nd AIAA International Space Planes and Hypersonics Systems and Technologies Conference*. American Institute of Aeronautics and Astronautics, sep 2018.

[17] M. W. Chase. NIST-JANAF Thermochemical Tables. *American Institute of Physics for the National Institute of Standards and Technology*, 1998.

[18] M. Selzer, S. Schweikert, H. Boehrk, H. Hald, and J. von Wolfersdorf. Comprehensive C/C sample characterizations for transpiration cooling applications. Technical report, Sonderforschungsbereich Transregio 40 - Annual Report 2016, pp. 61-72, 2016.

[19] H. Hald, A. Herbertz, M. Kuhn, and M. Ortelt. Technological aspects of transpiration cooled composite structures for thrust chamber applications. In *16th AIAA/DLR/DGLR International Space Planes and Hypersonic Systems and Technologies Conference*. American Institute of Aeronautics and Astronautics, oct 2009.

[20] H. Boehrk, V. Wartemann, T. Eggers, J. M. Schramm, A. Wagner, and K. Hannemann. Shock tube testing of the transpiration-cooled heat shield experiment AKTiV. In *18th AIAA/3AF International Space Planes and Hypersonic Systems and Technologies Conference*. American Institute of Aeronautics and Astronautics, sep 2012.

[21] T. Langener, J. von Wolfersdorf, M. Selzer, and H. Hald. Experimental investigations of transpiration cooling applied to c/c material. *International Journal of Thermal Sciences*, 54:70–81, apr 2012.

[22] T. Langener, J. von Wolfersdorf, and J. Steelant. Experimental investigations on transpiration cooling for scramjet applications using different coolants. *AIAA Journal*, 49(7):1409–1419, jul 2011.

[23] A. Herbertz, M. Ortelt, I. Müller, and H. Hald. Efficiency evaluation of transpiration cooled ceramic combustion chambers. *CEAS Space Journal*, 6(2):99–105, apr 2014.

[24] S. Schweikert, S. Loehle, M. Selzer, H. Boehrk, and J. von Wolfersdorf. Surface heat flux determination of transpiration cooled c/c by the application of non-integer system identification. In *8th European Workshop on Thermal Protection and Hot Structures*. ESA, 04 2016.